Essential Readings in Light Metals: Cast Shop for Aluminum Production.
Edited by John F. Grandfield and Dmitry G. Eskin.

A THERMODYNAMIC STUDY OF METASTABLE Al-Fe PHASE FORMATION IN DIRECT CHILL (DC)-CAST ALUMINUM ALLOY INGOTS

Celil A. Aliravci[1&2], John E. Gruzleski[1] and Mihriban Ö. Pekgüleryüz[2]

[1]Department of Mining and Metallurgical Engineering, McGill University
Montreal, Quebec, Canada

[2]Alcan-UQAC Chair in Solidification and Metallurgy of Aluminum
Department of Applied Sciences, University of Quebec in Chicoutimi
555 University Street, Chicoutimi, Québec, Canada G7H 2B1

Abstract

In direct-chill (DC)-cast 1xxx-and 5xxx-series Al sheet-ingots, the presence of mainly Fe and some Si, and cooling rates increasing from < 1°C/s in the ingot center to ~20°C/s near the surface cause the formation of metastable intermetallic Al_6Fe and Al_mFe compounds in addition to the stable Al_3Fe, and hence the *fir-tree* defect. Since the Al-Fe and Al-Fe-Si phase diagrams are not useful in predicting the metastable phase formation, a binary phase diagram study was conducted to calculate the Al-Al_6Fe and Al-Al_mFe metastable phase equilibria using a thermodynamic software and an Al-alloy database. The Al-Al_3Fe phase diagram was calculated using the existing Gibbs energy data which gives the eutectic point at 1.85wt% Fe and the eutectic temperature as 654°C. The missing Gibbs energy data for the metastable phases were estimated using substitutional and graphical methods and the phase diagrams were calculated. In the Al-Al_6Fe phase diagram, the eutectic temperature is depressed from 654°C (equilibrium) to 648°C and the eutectic point is shifted from 1.85wt% Fe to 3.4wt% Fe. In the Al-Al_mFe phase diagram, the eutectic temperature is 643°C and the eutectic point is at 4.6wt% Fe. The verification of the calculated eutectic temperatures was carried out by DSC measurements which were conducted on samples removed from Al-Fe alloy rods directionally grown in a Bridgman-type solidification furnace. A good agreement is observed between the calculated and measured values.

Introduction

The 1xxx-and 5xxx-series aluminium alloys (Table I) constitute the two major non-heat-treatable (NHT) alloy groups used in more than twenty percent of all the flat-rolled Al products [1]. When these alloys are used in the fabrication of offset quality lithographic sheets and plates, and anodizing quality architectural panels, they require microstructurally homogeneous surfaces for high-quality surface finishing [1-2]. Both alloy series contain Fe and Si as the main impurities (Table I). Under equilibrium solidification conditions (dT/dt < 0.015°C/s) [3-4], any iron present in Al in excess of its solid solubility limit (0.04 wt% Fe) forms a eutectic of α-Al primary phase and an intermetallic Al_3Fe phase between the α-Al dendrite arms [5]. However, during DC-casting of 1xxx-and 5xxx-series Al ingots, considerably different local cooling rates (dT/dt), varying from < 1°C/s near the ingot centre to ~20°C/s near the ingot surface, cause the formation of the metastable Al_mFe and Al_6Fe intermetallic phases in addition to the stable Al_3Fe phase (Table II) [6-8]. The etching characteristics of these two metastable phases are quite different and the alternate dark and light etching of these zones creates a defect called the *fir-tree zone (FTZ)* in DC-cast ingots (Fig. 1). When the ingots are scalped and rolled to have Al sheets and plates, this leads to the formation of longitudinal bands and streaks (a zebra structure) which creates a major surface quality problem (Fig. 1).

The mechanism of metastable Al-Fe phase formation is not yet well understood. There is a real need for a good fundamental understanding of the mechanism of the formation (nucleation and growth) of metastable intermetallics via both kinetic and thermodynamic (phase diagram) studies. It is often considered that at higher cooling rates, due to kinetic restrictions, there is not enough time for the atoms of an alloy to arrange themselves into a stable solid structure. Hence, the formation of a less regularly packed but kinetically favoured metastable structure occurs [9]. Even though the kinetics of formation predominates over the thermodynamics, using only the kinetic approach is not sufficient since the knowledge of atomic motion during solidification is scarce and it is difficult to predict which type of structure will be

Table I. Chemical Composition of Major Non-Heat Treatable Wrought Al Alloys [1].

Alloy	Element (wt%)							
	Fe max	Si max	Cu max	Mn max	Mg	Cr max	Zn max	Al min
AA1050	**0.4**	**0.25**	0.05	0.05	< 0.05	–	0.05	99.50
AA1100	*	*	0.2	0.05	–	–	0.10	99.00
AA5005	**0.7**	**0.3**	0.20	0.20	0.5-1.1	0.10	0.25	rem

*0.95 (Si + Fe)

Table II. Structure, Composition and Cooling Rate Data for the Al-Fe Phases [3,6-8].

Phase	State	Bravais Lattice; Spacegroup	Lattice Parameter	Element, wt%	Cooling Rate, dT/dt, °C/s
Al_3Fe ($Al_{13}Fe_4$)	stable	*C* -centered monoclinic; *C* 2/m	a = 15.49 Å b = 8.08 Å c = 12.48 Å β = 107.75°	Fe = 37.3* Fe = 36† Si = 1.6† Ni = 0.4†	<3* < 1†
Al_6Fe	meta-stable	*C* -centered orthorombic; Ccmm/Ccm2$_1$	a = 6.49 Å b = 7.44 Å c = 8.79 Å	Fe = 25.6	(1-3) < dT/dt < (10-20)
Al_mFe $4 < m < 4.4$	meta-stable	body centered tetragonal (b.c.t.)	a = 8.84 Å b = 21.60 Å	Fe = 32.8*† Si = 2.4† Ni= 0.3†	> 20* > 10†

*In pure binary Al-Fe alloys. †In Al-Fe-Si ternary alloys.

kinetically favoured [9]. Another way to study the metastable phase formation is the thermodynamic approach which was proposed by Cahn [10]. In this approach, rapid solidification is considered as a solidification process with relatively large undercoolings. This approach uses metastable phase diagrams to show the minimum undercoolings required for metastable phases to form. Hence, the objective of this study was to calculate the phase diagrams for the metastable Al-Fe phases using a thermodynamic calculation software, and to experimentally verify the calculated invariant (eutectic) temperatures via differential scanning calorimetry (DSC).

Phase Diagram Calculations

The phase diagram calculations were carried out using ThermoCalc, a thermodynamic calculation software developed at the Royal Institute of Technology, Sweden [11] and an aluminum alloy database (KPAL/AA12S) assembled by Kaufman [12]. In this study, the liquid and the fcc (α-Al) solid solution phases were treated as regular substitutional solutions. The molar Gibbs free energy of mixing, G_m, or formation, G_f (though they are used interchangeably, the former is preferred for the liquid and solid solution phases, and the latter for compounds), of each phase can simply be given as [13]

$$G_m = G^{id} + G^{xs} \quad (1)$$

where G^{id} (= $G^o - T\Delta S_m$) is the integral ideal molar Gibbs free energy of the solution [14], G^o (= $X_{Al}G^o_{Al} + X_{Fe}G^o_{Fe}$) the molar Gibbs free energy of the unmixed pure components [13-15] and G^{xs} (= ΔH_m) is the integral excess molar Gibbs free energy of the solution. Equation (1) can also be given as [13-14]

$$\Delta G_m = \Delta G^{id} + G^{xs} = -T\Delta S_m + \Delta H_m \quad (2)$$

where ΔH_m (=$X_{Al}X_{Fe}\Omega$) is the molar enthalpy of mixing, ΔS_m {= $R(X_{Al}\ln X_{Al} + X_{Fe}\ln X_{Fe})$} the molar entropy of

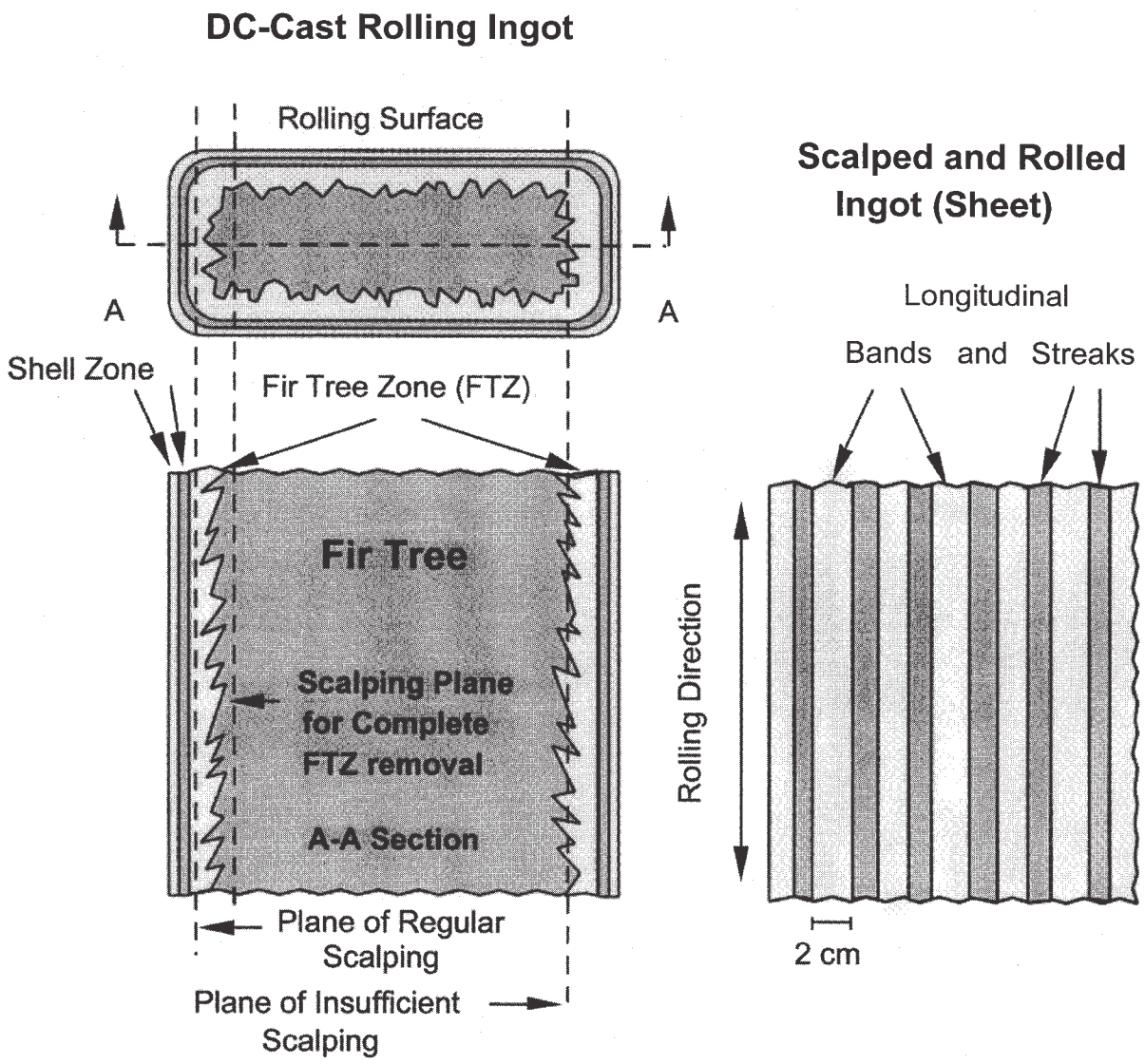

Figure 1: Schematic of different zones forming in DC-cast rolling ingots and the zebra structure (bands and streaks) forming in scalped and rolled ingot.

mixing, and T is the absolute temperature (K). Thus,

$$\Delta G_m = RT(X_{Al}\ln X_{Al} + X_{Fe}\ln X_{Fe}) + X_{Al}X_{Fe}\Omega \qquad (3)$$

where X_{Al} and X_{Fe} are mole fractions of Al and Fe, R the gas constant (8.3144 joule/degree.mole), and Ω the interaction coefficient describing the composition dependence of G^{xs}. The composition dependence (Ω) of the excess Gibbs energy (G^{xs}) of each phase is described with a power series. In this study, the Redlich-Kister model which exists in ThermoCalc was used. Hence, G^{xs} can be written as:

$$G^{xs} = X_{Al}X_{Fe}\,[L_0 + L_1(X_{Al} - X_{Fe}) + L_2(X_{Al} - X_{Fe})^2 + L_3(X_{Al} - X_{Fe})^3 + \ldots] \qquad (4)$$

where L_0, L_1, L_2, and L_3 are functions of temperature and pressure and describe the composition dependency of the binary parameters. The Al-Fe compounds (Al_3Fe, Al_6Fe and Al_mFe) are assumed to be line (stoichiometric) compounds, treated as pure species and also represented with Eq. (2). Furthermore, since there is no phase equilibrium between the Al_6Fe and Al_mFe phases, each phase should have a separate metastable phase diagram.

The Al_3Fe data exists in the Kaufman database as

$\Delta G_{f,\ Al_3Fe} = -27900 + 4.6*T$, but the missing Al_6Fe and Al_mFe data needed to be estimated. Since the Al_6Fe phase is isomorphous with the Al_6Mn (both are orthorombic with only ± 1.5% differences between their respective lattice parameters) and Fe and Mn are both first-series transition elements, the thermodynamic data that exists for one can be used for the other with some degree of caution [3]. However, for a better approximation, the Gibbs energy data which exists in the database for the $Al_6(Fe,Mn)$ phase was substituted for the Al_6Fe to calculate the Al-Al_6Fe phase diagram. In the $Al_6(Fe,Mn)$ phase, up to 64% Mn can be displaced by Fe with only slight changes in lattice parameters [3]. For this calculation, the Al_3Fe which has a lower ΔG_f value (more stable) had to be suppressed. The Gibbs free energy of formation for the $Al_6(Fe,Mn)$ is given as $\Delta G_{f,\ Al_6(Fe,Mn)} = -15000 + 2.5*T$.

To estimate the ΔG_f data for Al_mFe, a graphical approach was used (Fig. 2). Figure 2 is a plot of the enthalpy of formation vs composition (ΔH_f vs wt% Fe) for the Al-Fe binary system (data is from Hultgren [16]). The ΔH_f values for all the stable Al-Fe phases are represented by the ABC curve. Point B gives the ΔH_f for Al_3Fe as a line compound at 37.3wt% Fe. Placing the data for Al_6Fe as a line compound ($\Delta H_{f,\ Al_6Fe} = -15000$ at 25.7 wt% Fe) at point D on the the graph, a straight line, ADE, can also be drawn to approximate the partial ΔH_f vs wt% Fe curve for Al_6Fe and other phases that may (theoretically) form showing isometastability with Al_6Fe. Since Al_mFe is more metastable than Al_6Fe and requires a separate phase diagram, its ΔH_f value (and its partial ΔH_f vs wt% Fe curve) should lie above the ADE line. By drawing a straight vertical line from the 32.8wt% Fe point (Fe concentration for Al_mFe) and extending it above ADE line gives point G (found by trial and error calculations using various values above point F) which represents a good first estimate for the ΔH_f value of Al_mFe. The ΔS_f for Al_mFe was also calculated using the same approach on the ΔS_f vs wt% Fe graph (not shown). Hence, the free energy relationship for the Al_mFe phase was proposed to be

$$\Delta G_{f,\ Al_mFe} = -18750 + 3.15*T. \qquad (5)$$

DSC Measurements

For DSC measurements, two Al-Fe and one Al-Fe-Si alloy rod samples (2 mm dia. x 160 mm length) were grown in a Bridgman-type directional solidification furnace. The composition, growth parameters and the phases formed are given in Table III. The binary alloys (1&2) were prepared using super purity (>99.995%) Al and high-purity Al-5wt% Fe master alloy. The ternary alloy (3) was prepared from a remelted DC-cast AA1050 alloy ingot. The intermetallic phases removed from the samples by a matrix-dissolution method [17] were analyzed by XRD (Table III). The flat disc-shaped DSC specimens (0.5 mm thick and 2 mm in diameter) were removed from the central regions of the Bridgman-grown rods using a low-speed radial saw (Buehler Isomet 110) and a cooling liquid. Very small specimens (3 mg - 6 mg) were used to get a fast response, minimum thermal lag, high peak resolution and temperature accuracy [4]. The specimens were cleaned in acetone, placed in graphite pans and the measurements were carried out using a Perkin-Elmer DSC-7 system (a power compensation DSC) operating under dynamic nitrogen atmosphere. The system calibration was carried out by using a super-purity Al standard. Placing a specimen in the sample cell and an empty graphite crucible in the reference cell at 50°C, the calorimeter was quickly heated up (at a heating rate of 200°C/min) to ~640 °C and it was stabilized for 1 min at this temperature. Then, the temperature scan was performed at a linear and low heating rate of 1°C/min till the melting peak of α-Al was recorded. This rate was selected for better peak resolution and separation, and temperature accuracy [4]. All measurements were performed on three specimens taken from each sample. To minimize the undercooling, the scanning was performed only in the heating mode.

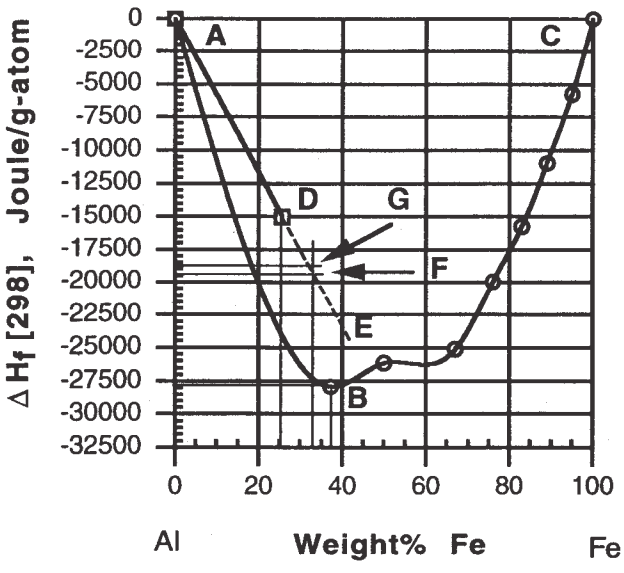

Figure 2: Enthalpy of formation vs composition relationship for the Al-Fe binary system.

Table III. Composition and Process Parameters for the Bridgman Samples, and XRD Results.

Sample No/Type	Fe, wt%	Si, wt%	Furnace Temp,°C	R, mm/min	G, °C/mm	dT/dt = GxR, °C/min (°C/s)	Major Phase	Minor Phase
1/AlFe	1.46	—	900	5	12	60 (1)	Al_3Fe	—
2/AlFe	1.46	—	900	50	12	600 (10)	Al_6Fe	—
3/AlFeSi	0.3	0.1	900	70	8-10	~630 (10.5)	Al_mFe	Al_6Fe

R = (Growth) **R**ate **G** = (Thermal) **G**radient **dT/dt** = Cooling rate

Results and Discussion

Figures 3-5 show the calculated binary phase diagrams for Al-Al_3Fe, Al-Al_6Fe and Al-Al_mFe (m = 4) equilibria and their enlarged Al-rich ends. The superposition of the enlarged Al-rich ends of the three phase diagrams is given in Fig. 6. It can be seen that as the equilibrium shifts from the stable (Al-Al_3Fe) to the most metastable (Al-Al_mFe), the eutectic temperature is depressed and the eutectic point is shifted to higher Fe levels (Table IV). Also, the solid solubility of Fe in Al increases with increasing metastability (Fig. 6).

The DSC heating (melting) thermograms for samples 1-3 containing Al-Al_3Fe, Al-Al_6Fe and Al-Al_6Fe/Al-Al_mFe eutectic phases (Table III) are shown in Figs 7-9. It can be seen that the Al-Al_3Fe, Al-Al_6Fe and Al-Al_mFe eutectic temperatures are measured to be 653.87°C (Fig. 7), 651.05°C (Fig. 8) and 645.35°C (Fig. 9), respectively. The symmetrical peaks characterizing the melting of Al-Al_3Fe and Al-Al_6Fe eutectics can easily be observed (Figs. 7-8,). Also, a small negative (exothermic) peak indicating the transformation of the metastable Al-Al_6Fe eutectic to the stable Al-Al_3Fe eutectic can be seen in Fig. 8.

A comparison of the eutectic temperatures obtained via the phase diagram calculations and DSC measurements is given in Table IV. Table IV also lists the data obtained by previous researchers. A good agreement is observed between the calculated and measured values within the accuracy ranges of the two methods: ~ ±1% for the ΔG_f data and ±0.1°C for the DSC measurements. The calculated Al-Al_3Fe eutectic temperature (654°C) agrees well with both the measured value obtained in the present work (653.87°C) and the measured value obtained by Lendvai (654.6°C) [19].

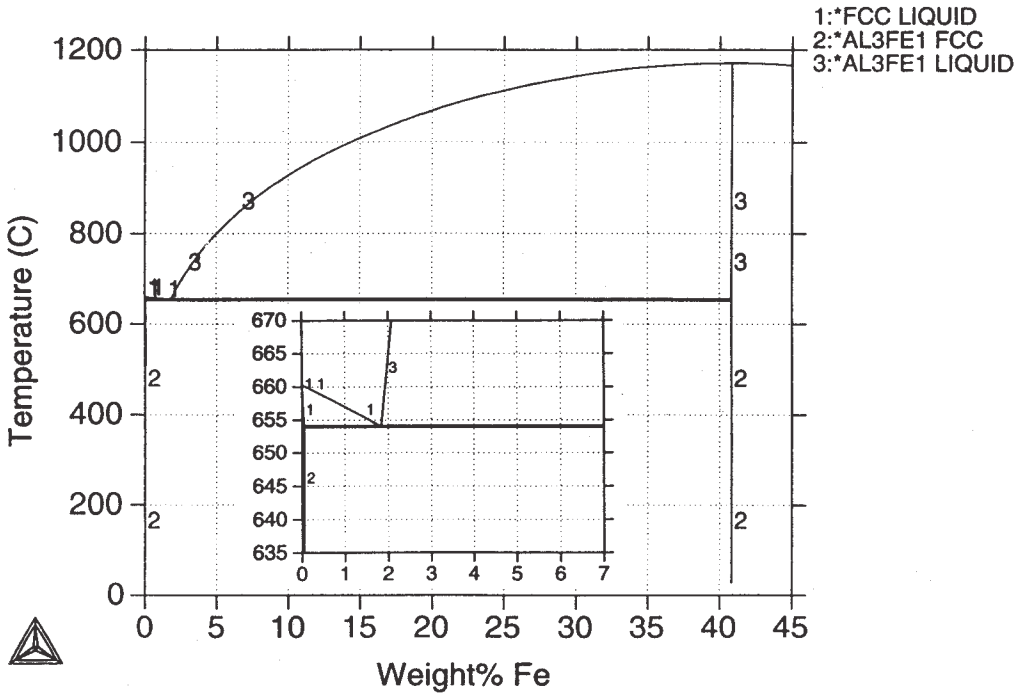

Figure 3: Al-Fe phase diagram computed for the Al-Al_3Fe equilibrium.

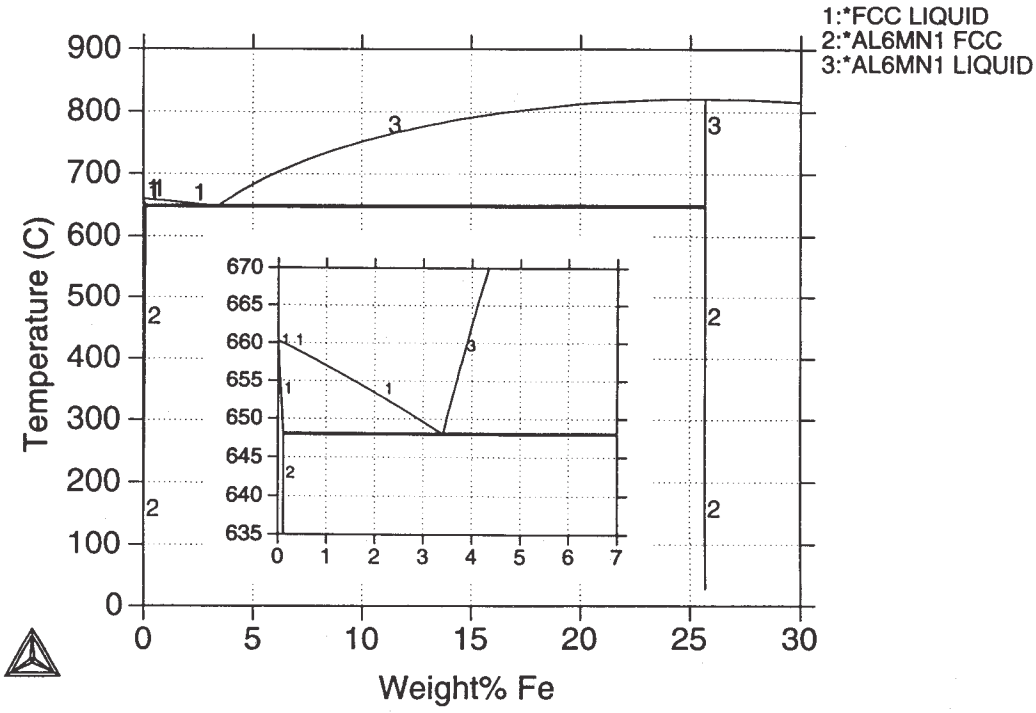

Figure 4: Al-Fe phase diagram computed for the Al-Al_6Fe equilibrium.

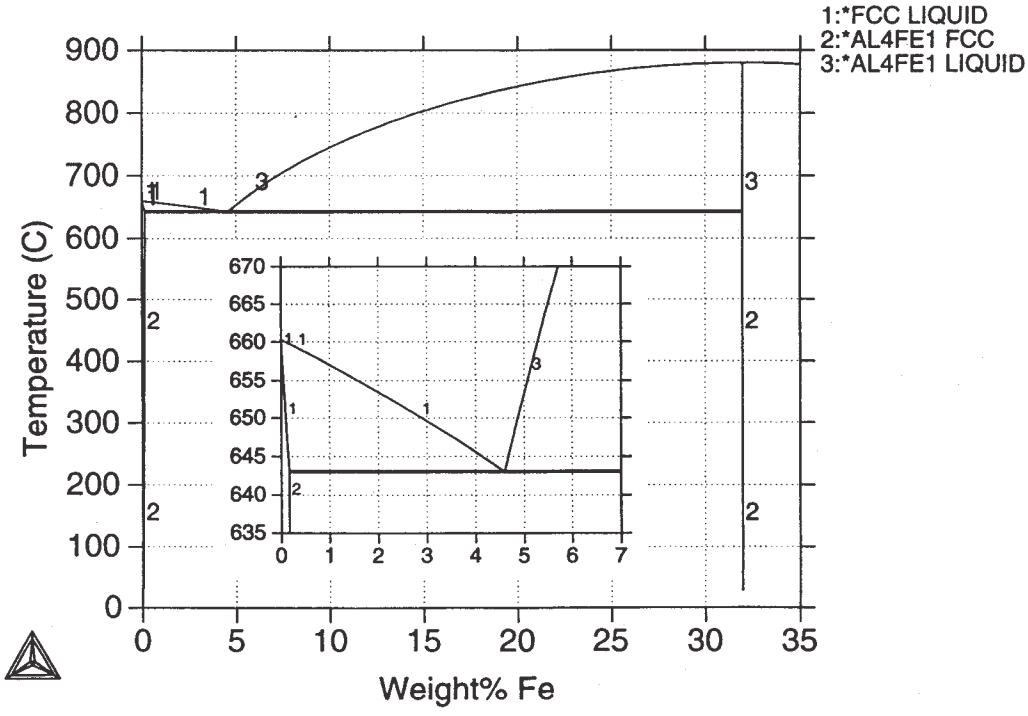

Figure 5: Al-Fe phase diagram computed for the Al-Al_mFe equilibrium.

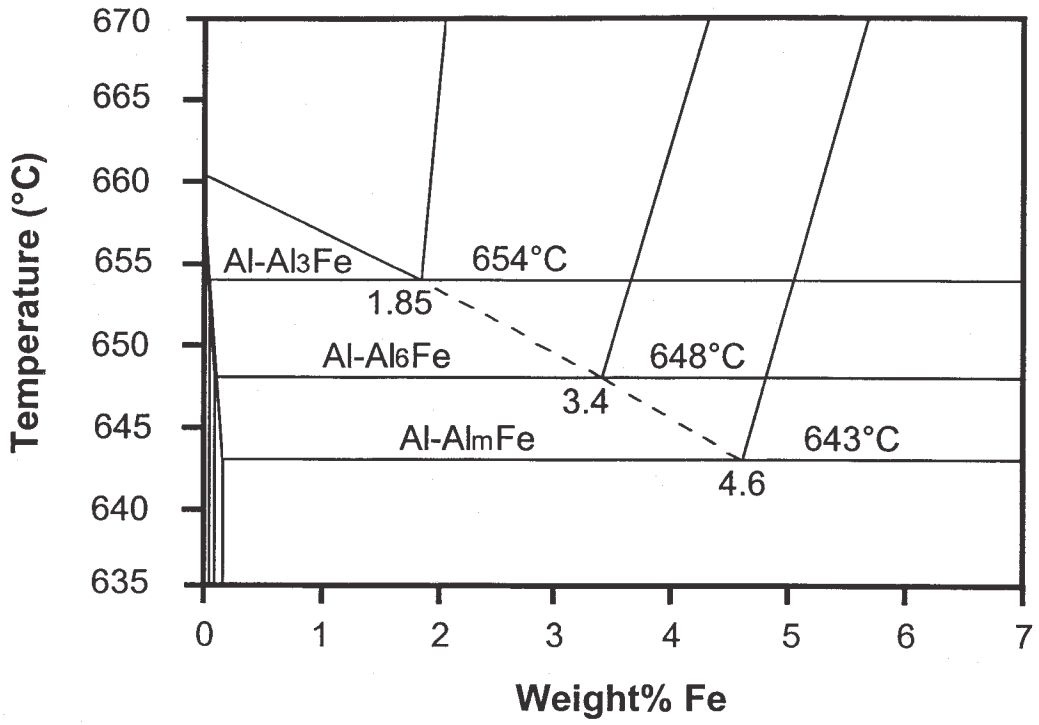

Figure 6: Superposition of the enlarged Al-rich ends of the stable and metastable Al-AlFe phase diagrams calculated via ThermoCalc.

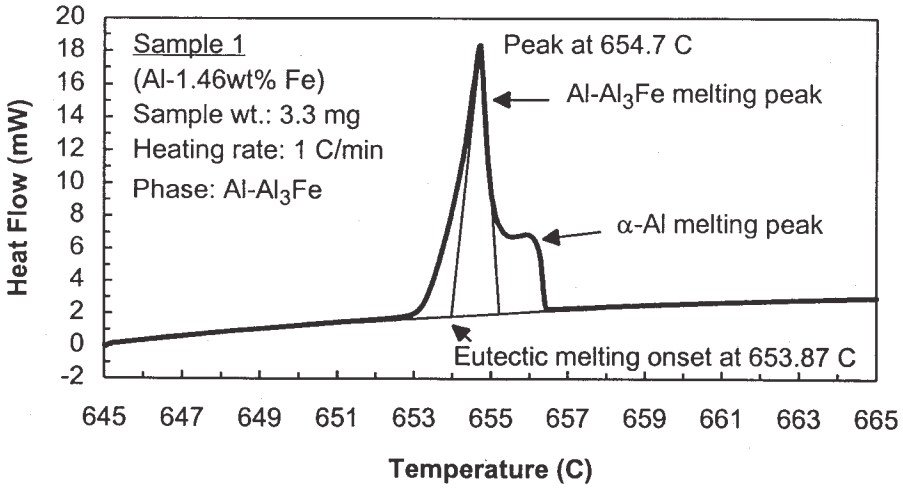

Figure 7: DSC heating thermogram for sample 1. The eutectic phase is 100% Al-Al_3Fe.

The calculated Al-Al_6Fe eutectic temperature and the measured value differ by ~3°C (Table IV). However, the calculated eutectic temperature (648°C) compares well with the DTA result (649°C) obtained by Perepezko [20]. Also, the measured value of 651.05°C compares well with both the DSC value (651.9°C) obtained by Lendvai [19] and the DTA value (649°C) obtained by Perepezko [20] (Table IV). The DSC results will provide a basis for the optimization of the calculated Al-Al_6Fe phase diagram.

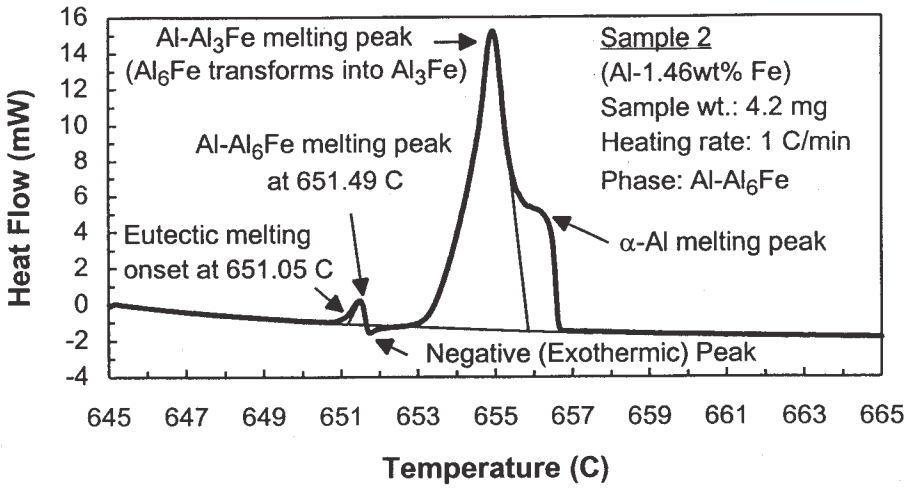

Figure 8: DSC heating thermogram for sample 2. The eutectic phase is 100% Al-Al_6Fe.

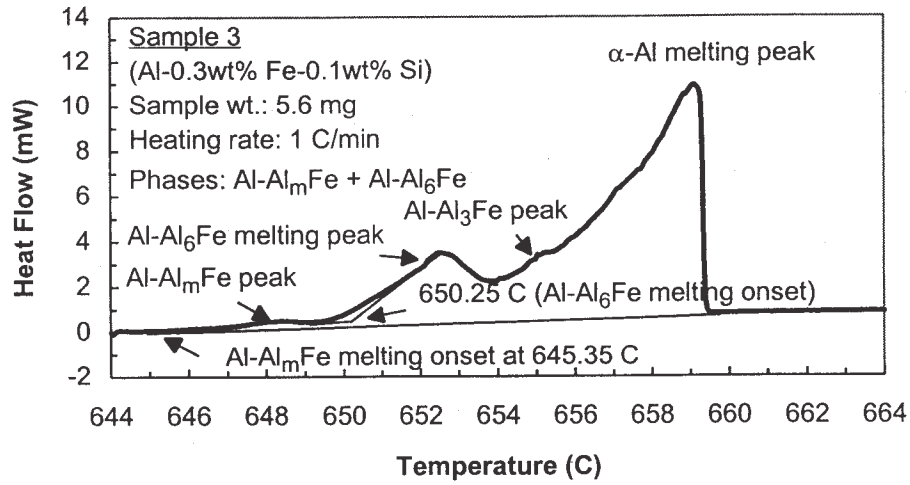

Figure 9: DSC heating thermogram for sample 3. Al-Al_mFe and Al-Al_6Fe eutectics coexist.

The calculated eutectic temperature for Al-Al_mFe (643°C) also compares well with the measured DSC value (645.35°C) (Table IV). There was neither any previous experimental thermodynamic data nor any phase diagram data for the Al_mFe phase. Therefore, the present phase diagram calculation and DSC measurement results for the Al-Al_mFe equilibrium cannot be evaluated comparatively. However, further DSC measurements will be carried out on samples containing the Al-Al_mFe eutectic and the results will be used towards the optimization of the Al-Al_mFe phase diagram.

Acknowledgments

The authors wish to express their sincere gratitute to the Natural Sciences and Engineering Research Council of Canada (NSERC), Alcan International Ltd. and the Foundation of the University of Quebec in Chicoutimi for providing the financial support. The authors are also grateful to Alcan International Ltd. Arvida Research and Development Centre (ARDC) for providing access to the Thermo-Calc software and Al alloy database. Also, Dr. Paul Evans of Alcan International Ltd. Banbury Laboratories (U.K.) is gratefully acknowledged for

Table IV. A Comparative Evaluation of Eutectic Temperatures Determined via Various Techniques.

Phase Equilibria	Eutectic Temperature Calculated via ThermoCalc, °C*	DSC Results, °C*†	Eutectic Temperature Calculated by Murray [18], °C	DSC by Lendvai [19], °C†	DTA by Perepezko [20], °C†
Al-Al_3Fe	654 (eut. at 1.85% Fe)	653.87	—	654.6	—
Al-Al_6Fe	648 (eut. at 3.4% Fe)	651.05	650 (eut at 3.2% Fe)	651.9	649
Al-Al_mFe	643 (eut. at 4.6% Fe)	645.35	—	—	—

*present study †eutectic melting onset temperature

providing the Bridgman-grown samples and XRD analyses. The authors would also like to thank Dr. Larry Kaufman for introducing them to ThermoCalc.

References

1. "Properties of Wrought Aluminum and Aluminum Alloys," Metals Handbook, vol. 2, S.R. Lampman et al., eds. (Metals Park, Ohio: ASM International, 10th ed., 1990), 62-122.
2. E.F. Emley, "Continuous Casting of Aluminium," Int. Met. Rev., Review 206, (June 1976), 75-115.
3. L. Bäckerud, "Kinetic Aspects of the Solidification of Binary and Ternary Alloy Systems" Jernkontorets Annaler, 152, (1968), 109-138.
4. W.Wm Wendlandt, Thermal Analysis, (New York , John Wiley & Sons, 1986), 662.
5. L.F. Mondolfo, Aluminium Alloys: Structure and Properties, (London: Butterworths, 1976), 283.
6. H. Kosuge and I. Mizukami, "Formation of Fir-Tree Structure in D.C. Cast Ingots of Al-0.6%Fe Alloys," J. Jap. Inst. L. Met., 25, (1975), 48-58.
7. H. Westengen, "Structure Inhomogeneities in Direct Chill Cast Sheet Ingots of Commercial Purity Aluminium," Aluminium, 07, (1982), 398-401.
8. P. Skjerpe, "Intermetallic Phases Formed During DC-Casting of an Al-0.25 Wt Pct Fe-0.13 Wt Pct Si Alloy," Met. Trans. A, 18A, (1987), 189-200.
9. P.H. Shingu, "Rapid Solidification and Metastable Equilibria in Light Metals," Light Metals: Science and Technology, C. Suryanarayana, P.M. Prasad, S.L. Malhotra and T.R. Anantharaman, eds. (Switzerland: Trans Tech, 1985), 77-83.
10. J.C. Baker and J.W. Cahn, "Thermodynamics of Solidification," Solidification, T.J. Hughel and G.F. Bolling, eds. (Metals Park, Ohio: American Society for Metals, 1971), 23-58.
11. B. Sundman, B. Jansson and Jan-Olof Andersson, "The Thermo-Calc Database System, " CALPHAD, 9, (1985), 153-190.
12. L. Kaufman, CAMSE 92, ed. M. Doyama, (Amsterdam: North-Holland, 1993), 1.
13. D.R. Gaskell, Introduction to the Thermodynamics of Materials, 3rd ed., (Bristol, PA: Taylor & Francis, 1995), 219-312.
14. P. Gordon, Principles of Phase Diagrams in Materials Systems, (New York, NY: McGraw-Hill, 1968), 46-106.
15. D.A. Porter and K.E. Easterling, Phase Transformations in Metals and Alloys, (London: Chapman & Hall, 1992), 1-59.
16. R.L. Hultgren, P.D. Desai, D.T. Hawkins, M. Gleiser and K.K. Kelley, Selected Values of the Thermodynamic Properties of Binary Alloys, (Metals Park, Ohio: American Society for Metals 1973), 156.
17. C.J. Simensen, P. Fartum and A. Andersen, "Analysis of Intermetallic Particles in Aluminium by Dissolution of the Sample in Butanol, " Fresnius Z. Anal. Chem., 319, (1984), 286-292.
18. J.L. Murray, "Thermodynamic Factors in the Extension of Solid Solubility in Al-Based Alloys," Mat. Res. Soc. Symp. Proc., 19, (Elsevier Science, 1983), 249-262.
19. J. Lendvai, G. Honyek, Zs. Rajkovits, T. Ungár, I. Kovács and T. Túrmezey, "The Properties of Al-Fe Ingots Cast at Different Casting Rates," Aluminium, 5, (1986), 363-366.
20. J.H. Perepezko, S.E. LeBeau, B.A. Mueller and G.J. Hildeman, Rapidly Solidified Powder Aluminum Alloys, eds. M.E. Fine and E.A. Starke, ASTM, (1986), 118.